IOP Publishing Journal of Physics: Condensed Matter
J. Phys.: Condens. Matter **32** (2020) 225703 (12pp) https://doi.org/10.1088/1361-648X/ab720d

Energetic, structural and electronic features of Sn-, Ga-, O-based defect complexes in cubic In_2O_3

Alexandr I Cocemasov[1], Vladimir I Brinzari[1] and Denis L Nika

Department of Theoretical Physics, E. Pokatilov Laboratory of Physics and Engineering of Nanomaterials, Moldova State University, Chisinau, MD 2009, Moldova

E-mail: dlnika@yahoo.com

Received 26 September 2019, revised 21 January 2020
Accepted for publication 31 January 2020
Published 3 March 2020

Abstract

Defect energy formation, lattice distortions and electronic structure of cubic In_2O_3 with Sn, Ga and O impurities were theoretically investigated using density functional theory. Different types of point defects, consisting of 1–4 atoms of Sn, Ga and O in both substitutional and interstitial (structural vacancy) positions, were examined. It was demonstrated, that formation of substitutional Ga and Sn defects are spontaneous, while formation of interstitial defects requires an activation energy. The donor-like behavior of interstitial Ga defects with splitting of conduction band into two subbands with light and heavy electrons, respectively, was revealed. Contrarily, interstitial O defects demonstrate acceptor-like behavior with the formation of acceptor levels or subbands inside the band gap. The obtained results are important for an accurate description of transport phenomena in In_2O_3 with substitutional and interstitial defects.

Keywords: In_2O_3, defects, electronic structure, density functional theory

(Some figures may appear in colour only in the online journal)

1. Introduction

Indium oxide is one of the basic transparent semiconducting metal oxides, whose advantages and unique properties have been demonstrated in widespread applications in micro- and optoelectronics, chemical sensors, catalysis, photovoltaics, thermoelectric devices, etc [1–3]. In spite of rather intensive fundamental studies some aspects of its physico-chemical, electronic and magnetic behaviour remain unclear and their understanding may serve for further developments in aforementioned and possibly new areas of application. The crystallographic complexity of cubic In_2O_3 lattice impedes studies and interpretation of its physical properties. Even primitive cell consists of 8 formula units, i.e. 40 atoms.

One of the characteristic features of In_2O_3 lattice is an existence of structural vacancies (SVs) which form a kind of voids in the crystal lattice. The proportion of such vacancies in the unit cell is equal to the number of formula units. Additionally, the presence of structural vacancies results in distortions of oxygen in the 1st shell surrounding indium atoms. These lattice sites differ from ordinary interstitial sites because they can be considered as a continuation of lattice nodes and are placed at positions of so-called 'missed' anions. Therefore, it seems that the nature and point defect formation due to the impurity atoms embedded in SVs should be different in comparison with ordinary interstitial sites. Gallium is one of the interesting and prominent candidates for doping of binary In–O, ternary In–X–O and quaternary In–X–Y–O oxide materials where X, Y = Zn or Sn [4, 5]. Experimental studies [6] of In_2O_3:Ga thick films with large grains in μm scale have showed a strong increase of electrical conductivity versus Ga additive increase (more than 1 order of magnitude at 8 at.% Ga). Within the concept of isovalent impurity substitution by III group element it is difficult to explain such behavior and donor-like effect of Ga atom. Moreover, a weak monotonic decrease with Ga concentration of fundamental band

[1] These authors contributed equally to this work.

gap (FBG) was observed. Thermal conductivity also demonstrates drastic decrease with Ga (~3 times of magnitude) and Sn doping in the same concentration range [6, 7] and there is a lack of unambiguous explanation of this drop. Strong dependence of thermal conductivity on the defect concentration is crucial for phonon engineering, i.e. tuning of thermal and/or electrical conduction of materials via modification of their phonon properties [8–10].

In this paper we theoretically investigate the electronic band structures, formation energies, partial charges and bond configurations of In_2O_3 structure with different point defects conformed by Sn, Ga and O atoms that include both In lattice nodes (substitutional defects) and also structural vacancies (interstitial defects) as a possible sites for an atom's inclusion. Hereafter we will refer to interstitial atoms as those located in structural vacancies. Employing density functional theory (DFT), we determine the geometrical and energetic (formation) parameters of these effects and their impact on the unit cell structure. We also analyze donor or acceptor behavior of these effects as well as defect-induced modification of the electronic band structure, Bader partial charges [11] and electronic density of states (DOS).

The reminder of the paper is arranged as follows. In section 2 we describe our computational model of In_2O_3 with various point defects. Discussions of defect energetics and bonds configuration are given in sections 3.1 and 3.2 respectively. Section 3.3 describes key-features of electronic band structure in In_2O_3 with point defects conformed by Sn, Ga and O atoms. Conclusions are given in section 4.

2. Computational details

All electronic calculations were performed within density functional theory formalism as implemented in the Quantum ESPRESSO first-principles simulation package [12, 13]. The generalized gradient approximation (GGA) for exchange-correlation functional of Perdew, Burke and Ernzerhof (PBEsol) [14] was used. The plane wave cutoff energy of 650 eV and $3 \times 3 \times 3$ k-point mesh of the Monkhorst–Pack type [15] were found sufficient to converge the total energy and atomic coordinates. A comparative study by Rasander and Moram [16] of different approximations to exchange-correlation functional over a range of semiconductors and insulators have shown that PBEsol is a distinct improvement over local density approximation (LDA) and GGA-PBE approximation when comes to structure properties (bond lengths, stresses, etc). In defected systems this advantage of PBEsol could be important, as one should first obtain a structurally well relaxed lattice containing the defects. Moreover, Buckeridge *et al* [17] have found for a vacancy containing In_2O_3 a less than 1% variation in both electron and hole concentrations when comparing results of PBEsol and hybrid functional calculations.

For local density of states (LDOS) and band structure calculations a finer $8 \times 8 \times 8$ k-point grid was employed. Using the supercell approach the defect-free In_2O_3 with bixbyite crystal structure (space group Ia-3) and with various point defects containing Sn, Ga and O impurity atoms were modeled. A 40-atoms primitive cell was chosen as a defect-free reference. Following the Wyckoff notation [18] the reference cell contains 4 indium atoms in position b, 12 indium atoms in position d, 24 oxygen atoms in position e and 8 SVs in position c. Both In(b) and In(d) atoms are surrounded by six oxygen atoms, while all O atoms are four-fold coordinated with indium. The position of b, d, e, and c sites in In_2O_3 lattice is shown in figure 1. It is seen that the c-sites provide the natural space to accommodate the interstitial atoms.

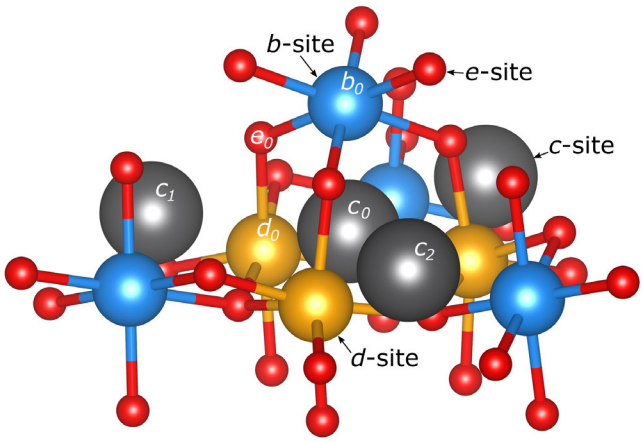

Figure 1. Schematic view of In_2O_3 lattice sites in the vicinity of b-site that is one of the corners of primitive unit cell. Blue nodes indicate In(b-site), yellow nodes show In(d-site), red nodes correspond to O(e-site), while gray sites indicate structural vacancy (c-site).

The In_2O_3 with various point defects was simulated by adding (removing) a certain number of In, O, Sn or Ga atoms to (from) the defect-free cell. The characteristic sites constituting the defects are marked in figure 1 as follows: b_0 and d_0 are b- and d-sites for substitutional atoms, c_0, c_1, c_2—c-sites for interstitial atoms, e_0—e-site for an oxygen vacancy. All cells were structurally relaxed until forces acting on the ions became below 0.01 eV Å^{-1} and internal stress decreased below 0.005 GPa. For pure In_2O_3 the equilibrium lattice constant was found to be $a = 10.157$ Å, only 0.4% larger than the experimental value 10.117 Å [19]. The calculated volumetric density was 7.04 g cm^{-3} that is about 2% less than experimental value 7.18 g cm^{-3} [20].

3. Results and discussion

3.1. Point defect energetics

Following the [21, 22] the formation energy (FE) of a neutral point defect can be obtained from DFT total energy calculations as:

$$E^{\mathrm{d}}_{\mathrm{form}} = E^{\mathrm{d}}_{\mathrm{tot}} - E^{0}_{\mathrm{tot}} - \sum_i n^{\mathrm{d}}_i \mu_i, \qquad (1)$$

where $E^{\mathrm{d}}_{\mathrm{tot}}$ is the total energy of a supercell calculation containing the defect, E^{0}_{tot} is the total energy of a defect-free supercell calculation, n^{d}_i is the number of atoms of type i that have been added to ($n^{\mathrm{d}}_i > 0$) or removed from ($n^{\mathrm{d}}_i < 0$) the supercell to form the defect, μ_i is the chemical potential of ith

Table 1. Formation energy.

Material	Formation energy, eV (*theory*)	Standard enthalpy of formation, eV (*experiment*)
In_2O_3	−10.0 (this work)	−9.47 [25–28]
SnO_2	−5.77 (this work)	−5.98 [25, 26]
Monoclinic β-Ga_2O_3 appears at $T > 800$ °C	−10.78 (this work)	−11.28 [25]
Orthorhombic ε-Ga_2O_3 most stable up to 800 °C	−9.44 (this work)	N.A.
Molecular oxygen	−5.29 [32]	−5.11 [24]

atom type. For complex defects containing several impurity atoms we have presented formation energy per one atom.

Within the thermodynamic approach chemical potentials of In, Sn, Ga and O can be expressed through thermochemical heats of phase formations for In_2O_3, SnO_2, Ga_2O_3 and O_2 using the following expressions:

$$2\mu_{In} + 3\mu_O = \Delta H_{In_2O_3}, \quad (2)$$

$$\mu_{Sn} + 2\mu_O = \Delta H_{SnO_2}, \quad (3)$$

$$2\mu_{Ga} + 3\mu_O = \Delta H_{Ga_2O_3}, \quad (4)$$

$$2\mu_O = \Delta H_{O_2}, \quad (5)$$

where $\Delta H_{In_2O_3}$, ΔH_{SnO_2}, $\Delta H_{Ga_2O_3}$ and ΔH_{O_2} are the respective heats of formation. Note, for exothermic reactions these values are negative. Each of equations (2)–(5) describes only the part of total thermochemical reaction—the formation process of the corresponding compound. This means that the rate of reverse process (decomposition) is too small and can be excluded from consideration. Otherwise, the establishment of equilibrium would lead to changes in the basic thermodynamic parameters of the system, including chemical potentials. Therefore, the sum of chemical potential values (left side of equations (2)–(5)) determines the transition boundary between the formation/decomposition of secondary phases only. The appearance of reverse reactions results in decomposition onset of secondary phases to their elementary phases. It occurs when the sum of chemical potentials exceeds the FE. In terms of interaction particles, the chemical potentials reflect the reservoirs for atoms that are involved in creating the substance and their values are also defined by experimental conditions. Naturally, at certain temperatures and pressures the chemical potentials of the same primary phases entering into different compounds have equal values.

At the same time these cohesive/formation energies for bixbyite In_2O_3, cassiterite SnO_2, ε-polymorph phase of Ga_2O_3 (orthorhombic phase) and molecular oxygen can be determined by the first-principles DFT approach as a difference between the total intrinsic electronic energies of indicated oxides and elementary phases participating in their formation i.e. In metal (space group 139, I4/mmm), Sn metal (space group 141, I41/amd), Ga metal (space group 64, Cmca) and O_2 molecule, respectively. Our approach based on equations (1)–(5) allows one to calculate formation energies of defects without introducing in the model of so-called 'metal rich'/'oxygen poor' and 'metal poor'/'oxygen rich' conditions imposed on In and O chemical potentials, respectively. The latter results in non-physically wide range of formation energies (see [23], where FE of an O-vacancy is ranged from −0.49 eV to +2.74 eV depending on the metal/oxygen limits). In fact, it introduces an empirical uncertainty associated with the 'technological' factor which is beyond the first-principles calculations.

Formation energies of metal oxides and defects calculated in this work employing Quantum ESPRESSO simulation package with PBEsol functional is presented in tables 1 and 2, respectively. Available experimental data from [24–28] are also presented for comparison. Due to significant overbinding of O_2 molecule within LDA/GGA approximations [29–31] the formation energy of O_2 calculated in this work using GGA-PBEsol is −8.3 eV that significantly deviates from −5.29 eV obtained using hybrid functional [32] or −5.11 eV determined experimentally [24]. Therefore, in our calculations of defects energy formation we used formation energy of molecular oxygen from [32] to correctly obtain the oxygen chemical potential. Small deviation between theoretical and experimental results provided in table 1 could be attributed to a temperature difference between theory ($T = 0$ K) and experimental conditions ($T = 298.15$ K).

Our value for FE of V_O, which is one of the most extensively studied defects in In_2O_3, is in accordance with those reported by Tanaka *et al* [33] (1.53 eV) and by Agoston *et al* [34] (1.2 eV). However, their FE values were obtained in strongly different O-rich and O-poor conditions, respectively. Since these limiting conditions were necessary attributes in their models of a defect formation, reconsideration of the characteristic value for oxygen chemical potential indicated in [33, 34] may be in order.

Besides the FEs of defects with different composition, table 2 contains the Bader partial charges for impurity and host atoms. Bader analysis demonstrates that atoms initially introduced as neutral transited to charged states after DFT calculation. Interestingly, the partial charges of host atoms are far from values of pure ionic states i.e. In^{3+} and O^{2-} determined by chemical formula. The Bader charges together with the analysis of band diagrams and the position of the Fermi level allow to confirm the electronic donor or acceptor nature of these impurities. The position of Fermi level, discussed in section 3.3 below, provide an additional confirmation of donor/acceptor nature of the defects.

As one can see from table 2 there is a correlation between the highest FE and lowest reducing/oxidation states in the case of single Ga/O interstitials. Probably, this correlation is related to large local distortions of the lattice due to additional point charge and under-coordinated orbitals of the defect.

Table 2. Defect formation energies[a,b].

Type of defect	Formation energy, eV	Formation energy, eV per atom	Bader charge of impurity atoms, electron charge	Average Bader charge of host atoms, electron charge
V_O	1.55	1.55		In = +1.78 O = − 1.24
Sn_b	− 0.17	− 0.17	+2.35	In = +1.83 O = − 1.24
Sn_d	− 0.11	− 0.11	+2.32	In = +1.83 O = − 1.24
Sn_b–Sn_d	0.47	0.235	+2.28; +2.25	In = +1.81 O = − 1.24
Sn_b–Sn_d–O_i	1.56	0.52	+2.38; +2.40; − 1.21	In = +1.86 O = − 1.23
Ga_b	− 0.39	− 0.39	+1.90	In = +1.86 O = − 1.24
Ga_d	− 0.28	− 0.28	+1.88	In = +1.86 O = − 1.24
Ga_b–Ga_d	− 0.71	− 0.36	+1.90; +1.88	In = +1.86 O = − 1.24
Ga_b–Ga_d–Ga_i	2.43	0.81	+1.79; +1.80; +1.02	In = +1.79 O = − 1.24
Ga_b–Ga_d–O_i	2.78	0.93	+1.89; +1.90; − 0.67	In = +1.86 O = − 1.21
Ga_i–O_i	3.95	1.98	+1.72; − 1.22	In = +1.83 O = − 1.23
Sn_b–Ga_d	− 0.40	− 0.20	+2.35; +1.86	In = +1.83 O = − 1.24
Sn_b–Ga_d–O_i	2.86	0.95	+2.40; +1.90; − 1.01	In = +1.86 O = − 1.22
Sn_b–Ga_i	3.73	1.87	+1.00; +1.34	In = +1.81 O = − 1.23
Sn_b–Ga_i–$2O_i$	5.69	1.42	+2.37; +1.79; − 1.20; − 1.21	In = +1.84 O = − 1.23
O_i	***4.58***	***4.58***	***− 0.94***	***In = +1.87 O = −1.21***
Ga_i	***3.65***	***3.65***	***+ 1.01***	***In = +1.79 O = −-1.23***
Ga_i–V_O	***4.67***	***2.34***	***+ 0.94***	***In = +1.71 O = −1.23***

[a] Three of processes are highlighted (in bold italic) as the most energetically unfavourable.
[b] In_2O_3 Bader charges: In = +1.86*e*; O = − 1.24*e*.

Bond length changes in the 1st atomic shell of these interstitials and increase of a unit cell volume indirectly confirm this assumption (see table 3).

Comparative analysis of defect FEs allows separating them into several groups depending on their values:

– defects with negative or close to zero FE $\leqslant$ 0; such defects consist of Sn or Ga substitutional atoms in the lattice sites *b* or *d*, they are formed either from single atoms (single substitution) or pairs of atoms of the same type (double substitution) or different type (mixed-type substitution); such FE indicate that formation of defect is spontaneous while the defects listed below require activation by external energy and in real conditions this can be achieved by temperature activation during the material growth;
– defects with low activation energies 0 < FE < 1 eV; such defects consist of the pair of metal atoms in lattice sites *b* and *d* and third O or Ga atom located in SV vicinity;
– defects with moderate activation energies 1 eV < FE < 2 eV; among these defects are Sn_b–Ga_i–$2O_i$, Sn_b–Ga_i and Ga_i–O_i, i.e. defects consisting of 2 or 3 filled SVs; in terms of FE magnitude these defects are also ordinary O-vacancies with FE = 1.55 eV;
– defects with high activation energies FE > 2 eV; they are represented as single SVs filled by O or by Ga atoms as well as Frenkel-type defect Ga_i–V_O; their formation are the most energetically unfavourable.

3.2. Bonds configuration

The information about bonds configuration around the defects in In_2O_3 is presented in table 3. Analyzing table 3, the following features in the defect geometry can be revealed:

- Sn or Ga substitution results in slight bond contraction with O atoms located in the 1st shell; the contraction is practically the same for both single and double substitution; in the case of Sn atoms it is about 3%; in the mixed case or double Ga substitution such relative distance changes to around 7%;
- introduction of a single O atom in SV together with double substitution of Sn atoms results in O_i shift toward Sn by ~6%–10% from the geometrical center of SV; mixed or double Ga substitution results in O_i shifts from *b*-site towards *d*-site with relative displacement from the geometrical center by ~35% and 20%, respectively, wherein the contraction between metal atoms and the 1st O shell are within 2%–13%;
- introduction of a single Ga atom in SV results in Ga_i relative shift ~17% from In_b and In_d atoms towards O nodes; Sn_b–Ga_i complex also demonstrates Ga_i shift from In_d towards O nodes (~40%) and additionally it is characterized by In_d atom shift towards Sn_d with corresponding bond contraction ~20%; the latter case is also characterized by the largest change in the unit cell volume (~4%); Sn_b-Ga_i complex with additional 2 O_i atoms positioned in neighbor SVs retains the specified behavior although with smaller Sn_b–In_d bond contraction;

Table 3. Bond lengths and unit cell volume[a].

Defect type	Neighbor pair	Bond length, Å	$\Delta L/L_{In_2O_3}$, %	V_{cell}, Å^3	$\Delta W_{In_2O_3}$, %
Pure In_2O_3	In(b)–O	2.18 (6)		523.89	
	In(d)–O	2.14 ÷ 2.23 (6)			
	In(b)–In(d)	3.81 (6)			
	In(b)–V(i)	2.35 (1)			
	In(d)–V(i)	2.33 (3)			
	O–V(i)	2.36 ÷ 2.42 (6)			
	V(i)–V(i)	3.59			
V_O				524.78	+0.17
$Sn_{In(b)}$	Sn(b)–O	2.11 (6)	− 3.21	527.05	+0.60
$Sn_{In(d)}$	Sn(d)–O	2.08 ÷ 2.16 (6)	− 2.80 ÷ − 2.70	527.01	+0.595
$Sn_{In(b)}$–$Sn_{In(d)}$	Sn(b)–O	2.12 ÷ 2.16 (6)	− 2.75 ÷ − 0.92	530.51	+1.26
	Sn(d)–O	2.09 ÷ 2.17 (6)	− 2.33 ÷ − 2.69		
$Sn_{In(b)}$–$Sn_{In(d)}$–O_i	Sn(b)–O	2.12 ÷ 2.21 (6)	− 2.75 ÷ +1.38	526.54	+0.51
	Sn(d)–O	2.09 ÷ 2.26 (6)	− 2.33 ÷ +1.35		
	Sn(b)–O(i)	2.21 (1)	− 5.96		
	Sn(d)–O(i)	2.09 (1)	− 10.3		
	In(d)–O(i)	2.18 (1)	− 6.44		
$Ga_{In(b)}$	Ga(b)–O	2.03 (6)	− 6.88	515.23	− 1.65
$Ga_{In(d)}$	Ga(d)–O	1.99 ÷ 2.12 (6)	− 7.01 ÷ − 4.93	515.48	− 1.61
$Ga_{In(b)}$–$Ga_{In(d)}$	Ga(b)–O	2.01 ÷ 2.09 (6)	− 7.80 ÷ − 4.13	506.93	− 3.24
	Ga(d)–O	1.97 ÷ 2.12 (6)	− 7.94 ÷ − 4.93		
$Ga_{In(b)}$–$Ga_{In(d)}$–Ga_i	Ga(b)–O	1.89 ÷ 2.22 (5)	− 13.3 ÷ +1.83	532.27	+1.60
	Ga(d)–O	1.89 ÷ 2.08 (5)	− 11.68 ÷ − 6.73		
	Ga(b)–Ga(i)	2.78 (1)	+18.3		
	Ga(d)–Ga(i)	2.63 (1)	+12.88		
	In(d)–Ga(i)	2.61 (1); 2.71 (1)	+12.02; +16.31		
$Ga_{In(b)}$–$Ga_{In(d)}$–O_i	Ga(b)–O	1.99 ÷ 2.17 (6)	− 8.72 ÷ − 0.46	515.31	− 1.64
	Ga(d)–O	1.91 ÷ 2.26 (6)	− 10.75 ÷ +1.35		
	Ga(b)–O(i)	3.28 (1)	+39.6		
	Ga(d)–O(i)	1.91 (1)	− 18.0		
	In(d)–O(i)	2.24 (1); 2.81 (1)	− 3.86; +20.6		
Ga_i–O_i	O–Ga(i)	1.85 ÷ 2.17 (5)	− 21.6 ÷ − 10.3	543.72	+3.79
	Ga(i)–O(i)	3.40 (1)	− 5.29		
	In(b)–Ga(i)	2.72 (1)	+15.74		
	In(d)–Ga(i)	2.73 ÷ 2.82 (3)	+17.17 ÷ +16.53		
	In(b)–O(i)	2.29 (1)	− 2.55		
	In(d)–O(i)	1.69 (1); 2.07 (1)	− 27.47; − 11.16		
$Sn_{In(b)}$–$Ga_{In(d)}$	Sn(b)–O	2.09 ÷ 2.13 (6)	− 4.13 ÷ − 2.29	518.73	− 0.98
	Ga(d)–O	1.98 ÷ 2.11 (6)	− 7.48 ÷ − 4.48		
$Sn_{In(b)}$–$Ga_{In(d)}$–O_i	Sn(b)–O	2.07 ÷ 2.14 (6)	− 5.05 ÷ − 1.83	521.49	− 0.46
	Ga(d)–O	1.90 ÷ 2.11 (6)	− 11.21 ÷ − 5.38		
	Sn(b)–O(i)	3.04 (1)	+29.4		
	Ga(d)–O(i)	1.90 (1)	− 18.45		
	In(d)–O(i)	2.19 (1); 2.33 (1)	− 6.0; 0		
$Sn_{In(b)}$–Ga_i	Sn(b)–O	2.28 (3)	+4.59	546.48	+4.31
	Sn(b)–Ga(i)	2.48 (1)	+5.53		
	O–Ga(i)	1.90 (3)	− 19.49 ÷ − 21.49		
	Sn(b)–In(d)	2.98 (3)	− 21.78		
	In(d)–Ga(i)	3.31 (3)	+42.06		
$Sn_{In(b)}$–Ga_i–$2O_i$	Sn(b)–O	2.03 ÷ 2.20 (6)	− 6.88 ÷ +0.92	546.27	+4.27
	Sn(b)–Ga(i)	2.81 (1)	+19.57		
	O–Ga(i)	1.87 ÷ 2.06 (5)	− 20.76 ÷ − 14.88		
	Sn(b)–In(d)	3.60 ÷ 3.67 (3)	− 5.51 ÷ − 3.67		
	In(d)–Ga(i)	2.70 ÷ 2.81 (3)	+5.88 ÷ +20.60		
O_i	***In(b)–O(i)***	***2.35 (1)***	***0***	***529.66***	***+ 1.10***
	In(d)–O(i)	***2.22 (3)***	***− 4.72***		
Ga_i	***O–Ga(i)***	***1.98 (3)***	***− 16.1 ÷ −18.2***	***543.00***	***+ 3.65***
	In(b)–Ga(i)	***2.69 (1)***	***+ 14.47***		
	In(d)–Ga(i)	***2.70 (3)***	***+ 15.88***		
Ga_i–V_O	***O–Ga(i)***	***1.94 ÷ 2.12 (3); 2.89 (1)***	***− 17.8 ÷ −12.40; +19.42***	***540.93***	***+ 3.25***
	In(b)–Ga(i)	***2.82 (1)***	***+ 20.0***		
	In(d)–Ga(i)	***2.65 ÷ 2.70 (3)***	***+ 13.73 ÷ +15.88***		

[a] The most energetically unfavourable processes are highlighted in bold italic.

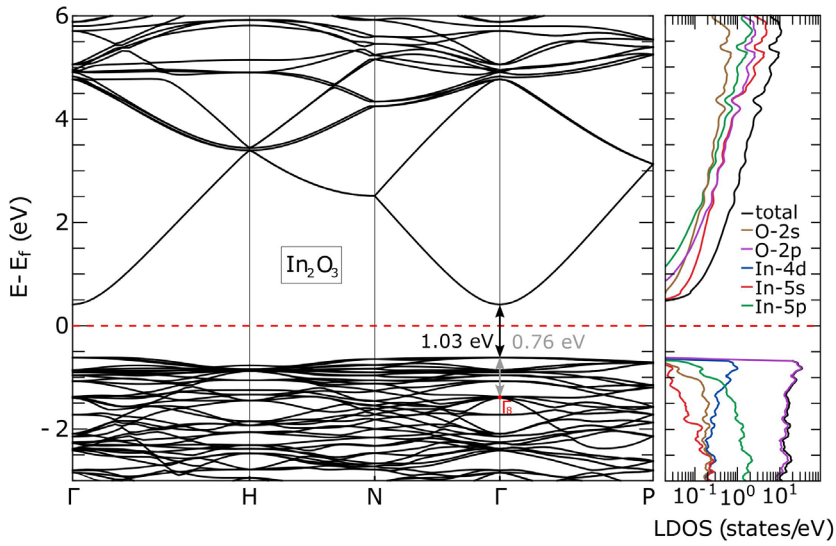

Figure 2. Defect-free In_2O_3 electronic band structure and LDOS with contribution from different orbitals. Fermi level is placed at 0 eV (dashed line). Γ_8-point shows valence band states responsible for the optical transitions.

- the defect totally constituted from 3 Ga atoms (Ga_b–Ga_d–Ga_i) is also characterized by Ga_i shift from *b*- and *d*-sites towards O nodes; its displacement is almost the same as for the single Ga_i defect.

It can be concluded that substitutional atoms weakly change the bond lengths and unit cell volume (within several %). The greatest distortions are observed in the case of interstitial Ga atoms. However, the real change in bond lengths near the defect does not exceed 12%. The highest enlargement of the unit cell volume can be explained quantitatively through the increase of Sn_b and Ga_i effective sizes due to their low oxidation states $Sn^{+1.0}$ and $Ga^{+1.34}$ according to the Bader partitioning. Stronger shifts revealed for some atomic positions which are related to interstitial atoms in SV only. The latter is a result of the rather free movement of interstitial atom within the SV cavity due to a lower coordination number and bond strength with nearest environment.

Introduction of interstitial Ga defects in In_2O_3 leads to a crystal lattice disorder. We can presume that the disorder induced by the rattling nature of interstitial atoms could strongly reduce the thermal conductivity of doped In_2O_3. Recent experimental results by Liu *et al* [6] on the significant drop of thermal conductivity in Ga-doped In_2O_3 indirectly confirm this assumption. Similar reduction of the thermal conductivity was found in other thermoelectric materials [35–39].

3.3. Electronic band structure

In our electronic calculations we have used the following valence configurations for atoms: O $2s^2 2p^4$, In $4d^{10} 5s^2 5p^1$, Sn $4d^{10} 5s^2 5p^2$ and Ga $3d^{10} 4s^2 4p^1$. Figure 2 shows calculated electronic band structure along Γ $(0,0,0)$-H $(1/2,-1/2,1/2)$-N $(0,0,1/2)$-Γ-P $(1/4,1/4,1/4)$ Brillouin zone path and the orbital-specific LDOS of pure In_2O_3.

We have considered the FBG as a difference in energies between the valence band maximum (VBM) and conduction band minimum (CBM). Our calculated FBG is 1.03 eV. Although this value is in a good accordance with other GGA-PBE calculations [40–42] it is much smaller than the values 2.7–3.2 eV obtained from experiments [43–49] and from more accurate DFT models with hybrid functionals [50, 51] or empirical Coulomb interaction parameters (DFT + U) [52]. The optical band gap (OBG) for pure In_2O_3 turns out to be larger than FBG due to the very low probability of photon absorption of interband direct optical transitions for the 1st (top) valence band (formally FBG transitions are forbidden). We estimated OBG as an energy distance between Γ_8 VB state and CBM (see [53] and figure 2). The obtained value of 1.79 eV is by 0.76 eV larger than FBG. This difference (denoted with gray arrows in figure 2) is close to values of 0.62 eV [44], 0.71 eV [54] and 0.8 eV [53] calculated from the hybrid functional and DFT + U calculations.

The FBG and OBG differ from each other, since in addition to the occupancy of electronic states optical transitions are affected by the selection rules and the corresponding transition probabilities. Due to the complexity of the In_2O_3 cubic lattice there is a set of bands in VB. The allowed optical transitions for the states of opposite parity between CBM and VBs were found at ~0.7–0.8 eV (bands state Γ_8 by Walsh *et al* [53] or Γ_{159}–Γ_{161} by Sabino *et al* [54]). Namely these transitions determine the OBG [53, 54].

The band structure details can be further analyzed from the LDOS calculations resolved for different orbitals. The upper part of the valence band (VB) shows a small dispersion and it is dominated by O 2p states with a weak overlap with In 4d and In 5p states. In the lowermost part of the first conduction band (CB) the In 5s states prevail. These states are characterized by a parabolic dispersion with an isotropic effective mass $m_x^* = m_y^* = m_z^* = 0.17 m_0$. For higher energies up to 5 eV with respect to CB minimum a strong hybridization between In 5s and O 2p states is found.

Band structures and orbital-dependent DOS for In_2O_3 with different point defects are presented in figures 3–5. The

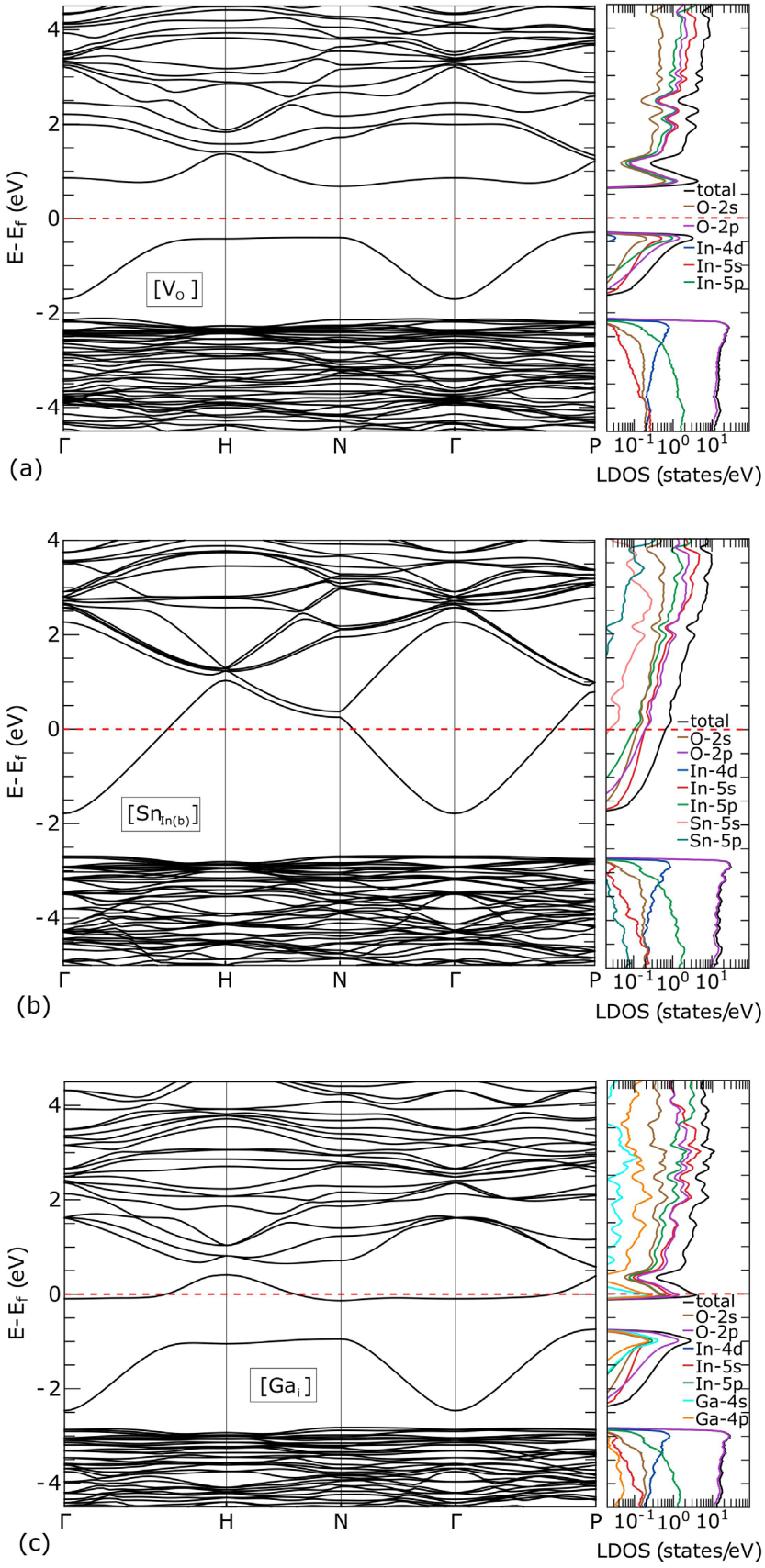

Figure 3. Electronic band structure and LDOS of indium oxide with one-site point defects: (a) V_O, (b) $Sn_{In(b)}$ and (c) Ga_i.

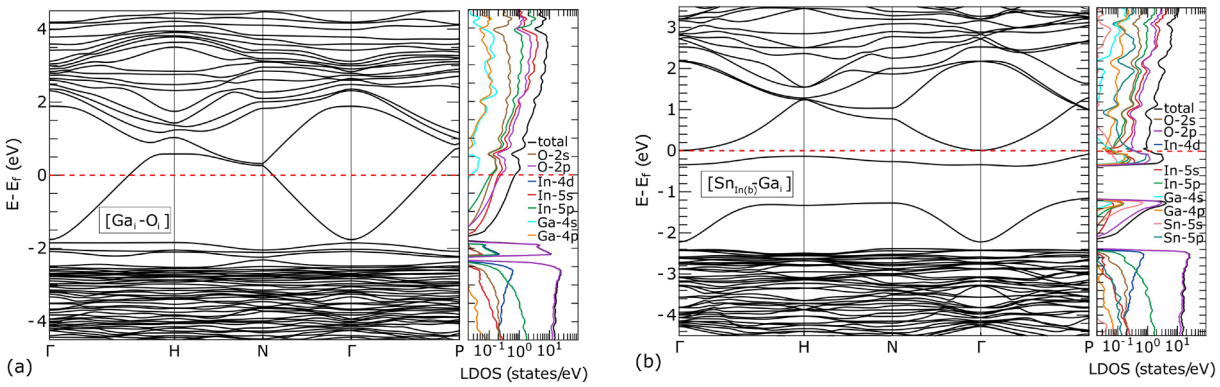

Figure 4. Electronic band structure and LDOS of indium oxide with two-site point defects: (a) Ga_i–O_i and (b) $Sn_{In(b)}$–Ga_i.

introduction of single $Ga_{In(b)}$ and $Sn_{In(b)}$ substitutions only weakly affects the band structure dispersion in comparison with pure In_2O_3. The major difference is the position of Fermi level, while for $Ga_{In(b)}$ case it remains inside the gap close to its center, for $Sn_{In(b)}$ it has climbed up to 1.76 eV above the bottom of CB (see figure 3(b)) turning the corresponding material into an n-type degenerate semiconductor. The introduction of an O vacancy (figure 3(a)) or an interstitial Ga (figure 3(c)) changes the band structure somewhat similarly, it splits the first CB into two subbands with a minimum energy gap in-between ~1 eV at point $N\,(0, 0, 1/2)$ of the Brillouin zone. For both these defects the Fermi level lies above the first subband manifesting strong donor behaviour. The LDOS of the first conduction subband revealed an overlap between oxygen and indium electronic orbitals with an additional mixing with Ga 4p and Ga 4s states in case of Ga_i defect. The second conduction subband is low-dispersive with minimum at $N\,(0, 0, 1/2)$ characterized by heavy electrons and by a pronounced peak in DOS. The LDOS analysis of this subband shows a strong mixing between O 2p, O 2s, In 5p and In 5s electronic states, again with some additional mixing with Ga 4p and Ga 4s orbitals for interstitial Ga defect. We note also, that for V_O defect the calculated value of ~1 eV for energy gap between two lowest conduction subbands is not far from 0.9 eV of Lu *et al* [50] obtained within a PBE + U method and from 0.91 eV of Melendez and Wierzbowska [55] obtained within LDA with self-interaction correction. Moreover, our additional calculation with GGA-PBE method [56] have revealed a very similar band structure for In_2O_3:V_O with maximal 5% difference at some parts of the Brillouin zone, as compared to GGA-PBEsol calculation.

The band structures of In_2O_3 with point defect complexes consisting of substitutions (Sn, Ga) and interstitials (Ga, O) in different combinations are more complicated (see figures 4 and 5). However, we conclude that some characteristic features described above for one-site defects are also found for defect complexes. Additionally, the introduction of oxygen interstitials is accompanied by appearance of numerous energy levels inside the band gap dominated by O 2p electronic states. Also, the largest deviation in electron effective masses of the first CB is found for Ga_i–O_i ($m_x^* = m_z^* = 0.15m_0, m_y^* = 0.14m_0$) and $Ga_{In(b)}$-$Ga_{In(d)}$-O_i ($m_x^* = 0.20m_0, m_y^* = m_z^* = 0.19m_0$) defect complexes. The electron effective masses for some distinctive cases of In_2O_3 with defect complexes along the selected symmetries are presented in table 4.

In general, the position of Fermi level itself reflects the changes of some part of total electron density and its redistribution in the CB or localization in the defect vicinity. In the first case, the Fermi level is located in the CB, whereas in the second case it is located in the band gap and reflects the formation of shallow or deep electronic levels. Bader partitioning can provide additional information on the electron density distribution over the lattice. It also may identify the donor/acceptor nature of electron levels located in the band gap. We will illustrate this for two characteristic defects. First defect is Sn_b, when according to electronic band structure the Fermi level lies in the CB. The second defect is Sn_b–Ga_d–O_i, when the Fermi level lies in the main forbidden zone.

- Sn_b case. The comparison of Bader partial charges between pure and defected In_2O_3 shows very small difference for all O atoms in both primitive cells and decrease of In (for all 15 atoms) partial charge from $\approx +1.86e$ (pure case) to $\approx +1.83e$ (defect case). Thus, charge acquired by In atoms for defect case is $q = +0.03e \cdot 15 = +0.45e$, which is almost equal (considering the simplicity of estimation) to the charge supplied by substituted Sn atom $q = +2.35e - 1.86e = +0.49e$. The free electron charge tends to concentrate near In sublattice and is repelled by O sublattice. Such kind of inhomogeneity in the electron distribution additionally suggests on a polar nature of the whole lattice. The same electron density pattern for ITO was obtained by Kim *et al* within VASP simulation package [57].
- Sn_b-Ga_d-O_i case. A more detailed look into Bader partitioning shows that the largest changes of partial charges occur in the 1st shell of the nearest cation and anion neighbors around the interstitial O, which possesses local charge of $-1.0e$. Atoms that contributed mostly to the compensation of O_i local charge are Sn_b, Ga_d, two In_d,

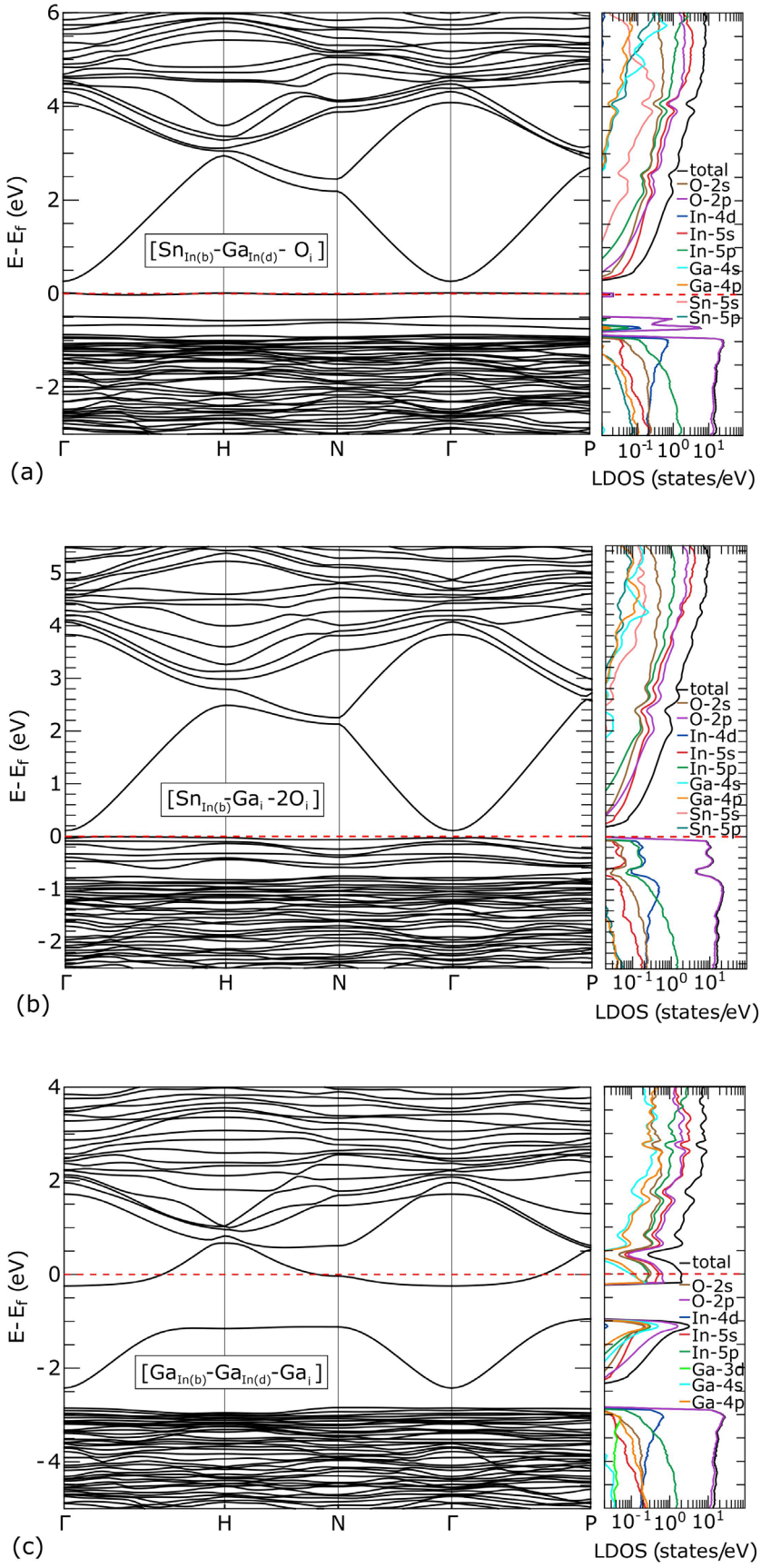

Figure 5. Electronic band structure and LDOS of indium oxide with three- and four-site point defects: (a) $Sn_{In(b)}$–$Ga_{In(b)}$–O_i, (b) $Sn_{In(b)}$–Ga_i–$2O_i$ and (c) $Ga_{In(b)}$–$Ga_{In(d)}$–Ga_i.

Table 4. Electron effective mass.

	Electron effective mass, m_0					
	$\Gamma \rightarrow$ P		$\Gamma \rightarrow$ N		$\Gamma \rightarrow$ H	
Type of defect	1st CB	2nd CB	1st CB	2nd CB	1st CB	2nd CB
Pure In_2O_3	0.17		0.17		0.17	
Sn_b	0.16		0.16		0.17	
Sn_b–Sn_d–O_i	0.16		0.16		0.16	
Ga_b–Ga_d	0.17		0.17		0.17	
Ga_b–Ga_d–O_i	0.19		0.19		0.20	
Ga_i	0.16	8.78	0.15	4.68	0.15	4.68
Ga_b–Ga_d–Ga_i	0.16	3.51	0.16	4.68	0.16	4.26

and two O atoms (all atoms are at distances in the range 1.9–3.04 Å (see table 3). The total charge compensation effect from these atoms is about $+0.9e$ and the rest of the charge ($+0.1e$) comes from the 2nd nearest shell.

Thus, the Bader analysis shows that both Sn substitutions and Ga interstitials lead to donor-type behaviour, while O interstitials result in acceptor-type behaviour and to appearance of band gap states. Moreover, donor-type behaviour should be accompanied by n-type conductivity because of the Fermi level position in the CB.

We have checked the consistency of our calculations in the case of single Sn_b substitution, using a relation between electron concentration n_{CB} in CB and defect concentration. As it follows from semiconductor statistics n_{CB} is a function of Fermi energy and CB effective mass. Single Sn_b substitution corresponds to doping of 6.25%, i.e. Sn concentration $n_{Sn} = 1.93 \cdot 10^{21}$ cm^{-3}. From our calculations we have obtained the following parameters of the CB: Fermi energy with respect to the CB $E_F - E_C = 1.76$ eV, electron CB effective mass $m_C^* = 0.17m_0$, CB charge gain due to the Sn_b charge loss during the In substitution $\Delta q_{CB} = 2.35e - 1.86e \cong 0.5e$ (see table 2). For degenerated semiconductor n_{CB} at $T = 0$ K is given by [58]:

$$n_{CB} = \frac{8\pi}{3}\left(\frac{2m_C^*(E_F - E_C)}{h^2}\right)^{3/2}. \quad (6)$$

Using equation (6) we estimate CB electron concentration as $n_{CB} = 7.4 \cdot 10^{20}$ cm^{-3}. Taking into account the released charge from Sn_b impurity, one can obtain the 'recalculated' Sn concentration as $1.48 \cdot 10^{21}$ cm^{-3} that is in reasonable accordance with aforementioned value of n_{Sn}.

The doping of In_2O_3 by Ga can considerably increase the electrical conductivity of material in spite of its isovalent impurity nature. This effect should be observable in the case of interstitial Ga. We did not calculate the electron concentration in the case of Ga_i defect due to the complexity of CB structure. However, the high position of Fermi level in CB (see figure 3(c)) gives the reason to assume that this value is comparable with n_e in ITO (Sn_b case). Increase of electrical conductivity in In_2O_3:Ga reported in [6] can be attributed to large number of Ga_i defects appearing in samples at high temperatures of oxide formation.

An accurate description of the electronic structure in In_2O_3 with different substitutional and interstitial impurities is important for an accurate quantitative description of electron-assisted processes, particularly for the calculations of electron-phonon interaction, electron scattering and electrical conductivity. The obtained electronic structure data are also necessary for a deeper study of electronic processes in In–Ga–Sn–O- and In–Ga–O-based metal-oxide semiconductor field-effect and thin film transistors, photosensitive and thermoelectric devices.

4. Conclusions

Within density functional theory approach the various point defect complexes in cubic In_2O_3 structure have been systematically studied. The considered defects were comprised from one to four atoms of Sn, Ga and O in substitutional and interstitial (structural vacancy) positions. The formation energies, Bader partial charges, bond configurations and electronic band structures were calculated and analyzed. The energies of defect formation were ranged from -0.7 eV to more than 4 eV, depending on the number of constituent atoms and their positions. It was demonstrated that defect formation energy can be calculated without introducing any ambiguous so-called technological factors using correct value of chemical potential of atomic oxygen determined from the formation energy of its molecular form. Substitutional Ga and Sn defects are the most energetically preferable and their formations are spontaneous, while Ga double-substitution complex has the lowest formation energy. Their isovalent and donating behaviour is explained within the traditional valence concept of substitutional doping.

The formation of interstitial atoms and their complexes requires an activation energy which usually decreases with the number of atoms comprising the complex. It was shown that interstitial Ga defects demonstrate donor-like behaviour and result in degenerated CB accompanied by its splitting into two subbands with light and heavy electrons. Contrariwise, interstitial O defects act as acceptors and lead to the formation of acceptor levels or subbands inside the band gap. These findings can shed light on unusually strong increase of electrical conductivity in In_2O_3 doped by Ga.

It was also revealed the decrease of CB effective mass for interstitial Ga defects and corresponding increase of CB effective mass for interstitial O defects. The calculation of electron LDOS for conduction subbands demonstrated an overlap between O and In electronic orbitals with an additional mixing with Ga 4p and Ga 4s states in the case of Ga_i defects. The obtained results are important for the interpretation of transport phenomena in In_2O_3 with different substitutional and interstitial defects. Physical properties of such defects could not be accurately described in the framework of the standard doping concept and density functional theory is required for both qualitative and quantitative predictions.

Acknowledgment

Authors acknowledge financial support from the Moldova State project #20.80009.5007.02. AIC acknowledges support under Moldova State project for young scientists #19.80012.02.13F.

ORCID iDs

Alexandr I Cocemasov https://orcid.org/0000-0001-9963-3817
Denis L Nika https://orcid.org/0000-0002-3082-3118

References

[1] Bierwagen O 2015 Indium oxide a transparent, wide-band gap semiconductor for (opto)electronic applications *Semicond. Sci. Technol.* **30** 024001
[2] Granqvist C G and Hultåker A 2002 Transparent and conducting ITO films: new developments and applications *Thin Solid Films* **411** 1–5
[3] von Wenckstern H, Splith D, Purfürst M, Zhang Z, Kranert Ch, Müller S, Lorenz M and Grundmann M 2015 Structural and optical properties of $(In,Ga)_2O_3$ thin films and characteristics of Schottky contacts thereon *Semicond. Sci. Technol.* **30** 024005
[4] Medvedeva J E and Hettiarachchi C L 2010 Tuning the properties of complex transparent conducting oxides: role of crystal symmetry, chemical composition, and carrier generation *Phys. Rev.* B **81** 125116
[5] Medvedeva J E, Buchholz D B and Chang R P H 2017 Recent advances in understanding the structure and properties of amorphous oxide semiconductors *Adv. Electron. Mater.* **3** 1700082
[6] Liu Y, Xu W, Liu D-B, Yu M, Lin Y-H and Nan C-W 2015 Enhanced thermoelectric properties of Ga-doped In_2O_3 ceramics via synergetic band gap engineering and phonon suppression *Phys. Chem. Chem. Phys.* **17** 11229–33
[7] Brinzari V, Cocemasov A, Nika D and Korotcenkov G 2017 Ultra-low thermal conductivity of nanogranular indium tin oxide films deposited by spray pyrolysis *Appl. Phys. Lett.* **110** 071904
[8] Balandin A A and Nika D L 2012 Phononics in low-dimensional materials *Mater. Today* **15** 266–75
[9] Cocemasov A I, Isacova C Ia and Nika D L 2018 Thermal transport in semiconductor nanostructures, graphene and related two-dimensional materials *Chin. Phys.* B **27** 056301
[10] Cocemasov A I, Nika D L, Fomin V M, Grimm D and Schmidt O G 2015 Phonon-engineered thermal transport in Si wires with constant and periodically modulated cross-sections: a crossover between nano- and microscale regimes *Appl. Phys. Lett.* **107** 011904
[11] Tang W, Sanville E and Henkelman G 2009 A grid-based Bader analysis algorithm without lattice bias *J. Phys.: Condens. Matter* **21** 084204
[12] Giannozzi P *et al* 2009 QUANTUM ESPRESSO: a modular and open-source software project for quantum simulations of materials *J. Phys.: Condens. Matter* **21** 395502
[13] Giannozzi P *et al* 2017 Advanced capabilities for materials modelling with quantum ESPRESSO *J. Phys.: Condens. Matter* **29** 465901
[14] Perdew J P, Ruzsinszky A, Csonka G I, Vydrov O A, Scuseria G E, Constantin L A, Zhou X and Burke K 2008 Restoring the density-gradient expansion for exchange in solids and surfaces *Phys. Rev. Lett.* **100** 136406
[15] Monkhorst H J and Pack J D 1976 Special points for Brillouin-zone integrations *Phys. Rev.* B **13** 5188
[16] Rasander M and Moram M A 2015 On the accuracy of commonly used density functional approximations in determining the elastic constants of insulators and semiconductors *J. Chem. Phys.* **143** 144104
[17] Buckeridge J *et al* 2018 Deep versus shallow nature of oxygen vacancies and consequent n-type carrier concentrations in transparent conducting oxides *Phys. Rev. Mater.* **2** 054604
[18] Wyckoff R W G 1922 *The analytical expression of the results of the theory of space-groups* (Carnegie Institution of Washington) p 180
[19] Marezio M 1966 Refinement of the crystal structure of In_2O_3 at two wavelengths *Acta Crystallogr.* **20** 723
[20] Lide D R (ed) 1986 *CRC Handbook of Chemistry and Physics* 67th edn (Boca Raton, FL: CRC Press) p B-95
[21] Van de Walle C G, Laks D B, Neumark G F and Pantelides S T 1993 First-principles calculations of solubilities and doping limits: Li, Na, and N in ZnSe *Phys. Rev.* B **47** 9425
[22] Freysoldt C, Grabowski B, Hickel T, Neugebauer J, Kresse G, Janotti A and Van de Walle C G 2014 First-principles calculations for point defects in solids *Rev. Mod. Phys.* **86** 253
[23] Hou Q, Buckeridge J, Lazauskas T, Mora-Fonz D, Sokol A A, Woodley S M and Catlow C R A 2018 Defect formation in In_2O_3 and SnO_2: a new atomistic approach based on accurate lattice energies *J. Mater. Chem.* C **6** 12386
[24] Ruscic B, Pinzon R E, Morton M L, von Laszevski G, Bittner S J, Nijsure S G, Amin K A, Minkoff M and Wagner A F 2004 Introduction to active thermochemical tables: several 'key' enthalpies of formation revisited *J. Phys. Chem.* A **108** 9979–97
[25] Lide D R (ed) 2009 *CRC Handbook of Chemistry and Physics* 90th edn (Boca Raton, FL: CRC Press)
[26] Haynes W M (ed) 2011 *CRC Handbook of Chemistry and Physics* 92nd edn (Boca Raton, FL: CRC Press) p 5.12
[27] Chase M W 1985 *JANAF Thermochemical Tables* 3rd edn (New York: American Institute of Physics) 1856
[28] Newns G R and Pelmore J M 1968 Thermodynamics of indium oxide from measurements of electromotive force *J. Chem. Soc.* A 360–2
[29] Jones R O and Gunnarsson O 1989 The density functional formalism, its applications and prospects *Rev. Mod. Phys.* **61** 689
[30] Patton D C, Porezag D V and Pederson M R 1997 Simplified generalized-gradient approximation and anharmonicity: benchmark calculations on molecules *Phys. Rev.* B **55** 7454
[31] Hammer B, Hansen L B and Norskov J K 1999 Improved adsorption energetics within density-functional theory using revised Perdew–Burke–Ernzerhof functionals *Phys. Rev.* B **59** 7413
[32] Ernzerhof M and Scuseria G E 1999 Assessment of the Perdew–Burke–Ernzerhof exchange-correlation functional *J. Chem. Phys.* **110** 5029
[33] Tanaka I, Oba F, Tatsumi K, Kunisu M, Nakano M and Adachi H 2002 Theoretical formation energy of oxygen-vacancies in oxides *Mater. Trans.* **43** 1426–9
[34] Agoston P, Albe K, Nieminen R M and Puska M J 2009 Intrinsic *n*-type behavior in transparent conducting oxides: a comparative hybrid-functional study of In_2O_3, SnO_2, and ZnO *Phys. Rev. Lett.* **103** 245501
[35] Slack G A and Tsoukala V G 1994 Some properties of semiconducting $IrSb_3$ *J. Appl. Phys.* **76** 1665–71
[36] Nolas G S *et al* 1998 Semiconducting Ge clathrates: promising candidates for thermoelectric applications *Appl. Phys. Lett.* **73** 178–80

[37] Nolas G S *et al* 1998 Effect of partial void filling on the lattice thermal conductivity of skutterudites *Phys. Rev.* B **58** 164–70
[38] Feldman J L, Singh D J, Mazin I I, Mandrus D and Sales B C 2000 Lattice dynamics and reduced thermal conductivity of filled skutterudites *Phys. Rev.* B **61** R9209
[39] Voneshen D J, Refson K, Borissenko E, Krisch M, Bosak A, Piovano A and Roger M 2013 Suppression of thermal conductivity by rattling modes in thermoelectric sodium cobaltate *Nat. Mater.* **12** 1028
[40] Karazhanov S Zh, Ravindran P, Vajeeston P, Ulyashin A, Finstad T G and Fjellvåg H 2007 Phase stability, electronic structure, and optical properties of indium oxide polytypes *Phys. Rev.* B **76** 075129
[41] Erhart P, Klein A, Egdell R G and Albe K 2007 Band structure of indium oxide: indirect versus direct band gap *Phys. Rev.* B **75** 153205
[42] Chen Z *et al* 2015 Electronic structures and transport properties of n-type-doped indium oxides *J. Phys. Chem.* C **119** 4789
[43] Scherer V, Janowitz C, Krapf A, Dwelk H, Braun D and Manzke R 2012 Transport and angular resolved photoemission measurements of the electronic properties of In_2O_3 bulk single crystals *Appl. Phys. Lett.* **100** 212108
[44] King P D C *et al* 2009 Band gap, electronic structure, and surface electron accumulation of cubic and rhombohedral In_2O_3 *Phys. Rev.* B **79** 205211
[45] Irmscher K, Naumann M, Pietsch M, Galazka Z, Uecker R, Schulz T, Schewski R, Albrecht M and Fornari R 2014 On the nature and temperature dependence of the fundamental band gap of In_2O_3 *Phys. Status Solidi* a **211** 54
[46] McLeod J A, Skorikov N A, Finkelstein L D, Kurmaev E Z and Moewes A 2012 Chemical bonding and hybridization in 5p binary oxide *J. Phys. Chem.* C **116** 24248
[47] de Boer T, Bekheet M F, Gurlo A, Riedel R and Moewes A 2016 Band gap and electronic structure of cubic, rhombohedral, and orthorhombic In_2O_3 polymorphs: experiment and theory *Phys. Rev.* B **93** 155205
[48] Braun D, Scherer V, Janowitz C, Galazka Z, Fornari R and Manzke R 2014 In-gap states of In_2O_3 single crystals investigated by scanning tunneling spectroscopy *Phys. Status Solidi* a **211** 59
[49] Schmidt-Grund R, Krauß H, Kranert C, Bonholzer M and Grundmann M 2014 Temperature dependence of the dielectric function in the spectral range (0.5–8.5) eV of an In_2O_3 thin film *Appl. Phys. Lett.* **105** 111906
[50] Fuchs F and Bechstedt F 2008 Indium-oxide polymorphs from first principles: quasiparticle electronic states *Phys. Rev.* B **77** 155107
[51] Zhang K H L, Lazarov V K, Veal T D, Oropeza F E, McConville C F, Egdell R G and Walsh A 2011 Thickness dependence of the strain, band gap and transport properties of epitaxial In_2O_3 thin films grown on Y-stabilised ZrO_2(1 1 1) *J. Phys.: Condens. Matter* **23** 334211
[52] Lu Y-B, Yang T L, Ling Z C, Cong W-Y, Zhang P, Li Y H and Xin Y Q 2015 How does the multiple constituent affect the carrier generation and charge transport in multicomponent TCOs of In–Zn–Sn oxide *J. Mater. Chem.* C **3** 7727
[53] Walsh A *et al* 2008 Nature of the band gap of In_2O_3 revealed by first-principles calculations and x-ray spectroscopy *Phys. Rev. Lett.* **100** 167402
[54] Sabino F P, Oliveira L N, Wei S-H and Da Silva J F 2017 Optical and fundamental band gaps disparity in transparent conducting oxides: new findings for the In_2O_3 and SnO_2 systems *J. Phys.: Condens. Matter* **29** 085501
[55] Melendez J J and Wierzbowska M 2016 In_2O_3 doped with hydrogen: electronic structure and optical properties from the pseudopotential self-interaction corrected density functional theory and the random phase approximation *J. Phys. Chem.* C **120** 4007
[56] Perdew J P, Burke K and Ernzerhof M 1996 Generalized gradient approximation made simple *Phys. Rev. Lett.* **77** 3865
[57] Kim S *et al* 2018 Transparent amorphous oxide semiconductor as excellent thermoelectric materials *Coatings* **8** 462
[58] Blakemore J S 1987 *Semiconductor Statistics* (New York: Dover) 381